Received 23 April 2023; revised 8 June 2023; accepted 1 July 2023. Date of publication 11 July 2023; date of current version 28 July 2023.

Digital Object Identifier 10.1109/OJCOMS.2023.3293330

Permutation Polynomial Interleaved DFT-s-OFDM

FREDRIK BERGGREN (Senior Member, IEEE), AND BRANISLAV M. POPOVIĆ

Huawei Technologies Sweden AB, 164 94 Kista, Sweden

CORRESPONDING AUTHOR: F. BERGGREN (e-mail: fredrik.b@huawei.com)

ABSTRACT We propose frequency-domain interleaver for discrete Fourier transform spread orthogonal division multiplexing (DFT-s-OFDM) based on a linear- or quadratic permutation polynomial (LPP/QPP). Interleaving the Fourier coefficients (i.e., the DFT precoder output) implies that the modulation symbols become transmitted over both time- and frequency domain, which is beneficial over time-frequency selective channels. Despite that the single-carrier property is lost due to the interleaving, the peak-to-average-power ratio (PAPR) can be improved. The results show that a QPP can suppress the error floor of the bit/block error rate (BER/BLER) which occurs on channels with large Doppler spread and simultaneously reduce the PAPR. An LPP primarily decreases the PAPR, especially for BPSK, where the gain is several dB. We derive criteria of how to analytically determine the QPPs and the LPPs.

INDEX TERMS Discrete Fourier transform spread orthogonal division multiplexing (DFT-s-OFDM), interleaver, permutation polynomial.

I. INTRODUCTION

RELIABLE communications over channels with high mobility is an important feature of cellular systems and an active area of research [1], [2]. In particular, waveforms which perform well in such scenarios, e.g., for high speed trains, satellites [3] etc., are of interest for 5G systems because communications at velocities up to 350 km/h should be supported, and in some cases even as high as 500 km/h [4]. Thereto, higher frequency bands are introduced in 5G compared to 4G systems, which further exacerbates the Doppler effect. Orthogonal frequency division multiplexing (OFDM) and discrete Fourier transform spread OFDM (DFT-s-OFDM) are used in both 4G Long Term Evolution (LTE) and 5G New Radio (NR), where DFT-s-OFDM is confined to uplink transmission. It has been proposed to introduce DFT-s-OFDM in the downlink for sub-THz communications [5], [6], [7]. OFDM multiplexes modulation symbols in the frequency domain by dividing the frequency spectrum into subcarriers. DFT-s-OFDM, on the other hand, is a single-carrier waveform which multiplexes modulation symbols in the time domain. Since a modulation symbol is transmitted over the whole frequency spectrum, performance may be better than for OFDM on a frequency selective channel. For OFDM, a modulation symbol is transmitted over the whole OFDM symbol and performance may be better than DFT-s-OFDM on a time selective channel.

Performance improvements for DFT-s-OFDM have been achieved by filtering the Fourier coefficients, i.e., the DFT precoder output. One direction is unitary frequency domain filtering, i.e., the filter only consists of phase rotations and is applied after the DFT precoder [8], [9]. The filter implies that the single-carrier property of DFT-s-OFDM is lost and the net effect is that a modulation symbol becomes transmitted over both time- and frequency domain. The benefit of these waveforms is that they have been shown to outperform OFDM and DFT-s-OFDM in bit/block error rate (BER/BLER) on a fading channel with large Doppler spread. Another direction is non-unitary frequency domain filtering, which is used for frequency domain spectrum shaping (FDSS), primarily to reduce the peak-to-average-power-ratio (PAPR) [10], [11], [12], [13]. With FDSS, the Fourier coefficients are multiplied with a window function which in turn smoothens the amplitude of the signal. The cost of the FDSS is typically a reduced spectral efficiency and that a larger signal-to-noise ratio (SNR) is required to maintain a given error rate. Furthermore, both non-unitary [14] and unitary FDSS [8] were suggested to generate chirp-based waveforms from DFT-s-OFDM, while also other methods to produce chirp-based waveforms have been considered [15]. These chirp-based waveforms can also improve performance on time-frequency selective channels.

Another way of manipulating the Fourier coefficients was proposed in [16], utilizing frequency domain interleaving, i.e., the DFT precoded symbols are interleaved. Thus, the single carrier property is lost and there is a potential performance gain over DFT-s-OFDM on a time-frequency selective channel. The benefit of this method is its simplicity, no filter is needed, and since DFT-s-OFDM is already implemented in existing 4G/5G systems, introducing interleaving after the DFT precoder could be a rather straightforward add-on. The existing parts of the transmit/receive chain could be kept and there would be no significant increase of the implementation complexity. On the other hand, the full potential of frequency domain interleaving is unclear, since prior work used random interleaving and no insight was provided on how to design the interleaver. Thus, it is an open issue how a particular interleaver affects either the BER/BLER or the PAPR. In [17], a block interleaver was utilized to interleave modulation symbols from different OFDM symbols, which is different from [16].

A sequence of randomly permuted integers could be used to interleave the Fourier coefficients [16], however, its performance impact is unpredictable. In an average sense, especially if the permutation sequence is long, random permutations may lead to improved BER/BLER. However, as will be shown herein, some permutation sequences do not improve the BER/BLER but improve the PAPR, and vice versa. Hence, within the set of permutation sequences, there are both 'good' ones and 'bad' ones, depending on the desired performance measure, e.g., BER/BLER or PAPR. Therefore, the performance of random interleaving can generally not be predicted or guaranteed. This leads us to consider interleavers based on permutation polynomials, which by their algebraic construction could be determined to result in desirable signal properties. A second issue with random interleaving is its implementation complexity. The interleaving sequence from a permutation polynomial could be computed in real-time since it is represented by a closed-form expression. However, a pseudo-random interleaver does not necessarily have any simple analytical structure and the permutation sequence may need to be stored in memory in the transmitter. A corresponding deinterleaver sequence will be stored in the receiver. An interleaver based on a permutation polynomial, on the other hand, can be fully and succinctly characterized by its polynomial coefficients, which requires less memory.

In this work, we propose the novel use of permutation polynomials for frequency domain interleaver for DFT-s-OFDM. A main benefit of this technique is that it is practically applicable and can be introduced into existing LTE and NR systems. The results show that interleaving can improve the BER/BLER on channels with large Doppler spread and can reduce the PAPR. The main contributions are summarized as follows:

- Selection of quadratic permutation polynomial (QPP): We derive a criterion for determining QPPs which improve the BER/BLER compared to DFT-s-OFDM. Prior methods for filtered DFT-s-OFDM may enhance either BER/BLER or PAPR, i.e., they are not improved simultaneously. In this work, we demonstrate that it is possible to enhance BER/BLER and PAPR simultaneously and a QPP can perform better than random interleaving.
- Selection of linear permutation polynomial (LPP): We derive a criterion for determining LPPs which improve the PAPR, especially for BPSK, compared to DFT-s-OFDM.
- Signal properties: We express frequency domain interleaved DFT-s-OFDM as a waveform with orthogonal basis functions. In contrast to those obtained by random interleaving, the basis functions are characterized by being sparse, i.e., contain many zero samples, and the sparsity is determined by the properties of the permutation polynomial. Moreover, we show that the property of ideal periodic autocorrelation is invariant under any permutation.
- Implementation aspects: We show that frequency domain interleaving can equivalently be represented as a linearly precoded DFT-s-OFDM signal. Furthermore, by decomposing the QPP, we determine several ways of generating the permutations to provide implementations with reduced complexity.

The rest of the paper is organized as follows. Section II gives the system model and we analyze properties of the interleaved DFT-s-OFDM signal. Based on these insights, Section III focuses on constructing permutation polynomials for reducing BER/BLER and PAPR, respectively. Implementation aspects are discussed in Section IV and the conclusions are drawn in Section V.

Notation: Throughout the paper, vectors are denoted by bold lowercase letters and matrices are denoted by bold uppercase letters, $\mathbf{I}$ is the identity matrix, $(\cdot)'$ and $(\cdot)^\dagger$ indicate the transpose and Hermitian transpose operators, respectively. The modulo-M operator is denoted by $(\text{mod}\, M)$, $\gcd(x, y)$ gives the greatest common divisor of x and y and $\arg(z)$ gives the angle of z. The conjugate operator is denoted by $(\cdot)^*$, and $\lfloor\cdot\rfloor$ and $\lceil\cdot\rceil$ indicate the floor and ceiling operators, respectively. $\delta[k]$ corresponds to the Kronecker delta function satisfying $\delta[0] = 1, \delta[k] = 0$ for all $k \neq 0$ $u(x)$ is the unit step function and $j = \sqrt{-1}$.

II. FREQUENCY DOMAIN INTERLEAVED DFT-S-OFDM

A. SIGNAL DEFINITION

We consider interleavers based on permutation polynomials and

$$\pi[k] = f[k] \,(\text{mod}\, M) \tag{1}$$

for $k = 0, 1, \ldots, M-1$ with

$$f[k] = f_p k^p + f_{p-1} k^{p-1} + \ldots + f_0 \tag{2}$$

is a pth degree permutation polynomial if it permutes the integers in the set $\{0, 1, \ldots, M-1\}$. The coefficients f_i are integers and it can be assumed that $f_i \in \{0, 1, \ldots, M-1\}$

since $\pi[k]$ has period M. It is known that there exists at least one inverse permutation polynomial, $\pi^{-1}[k]$, to each permutation polynomial, such that $\pi^{-1}[\pi[k]] = k$, cf. [18], [19]. Let $x[m], m = 0, 1, \ldots, M-1$, be the modulation symbols which could be, e.g., data carried by pulse amplitude modulated (PAM) or quadrature amplitude modulated (QAM) symbols, or consist of predetermined reference symbols or be symbols of a synchronization sequence. The modulation symbols are DFT precoded as

$$X[k] = \frac{1}{\sqrt{M}} \sum_{m=0}^{M-1} x[m] e^{-j\frac{2\pi}{M}mk}. \tag{3}$$

We define the interleaver using the permutation polynomial $\pi[k]$ which is applied to $X[k]$ such that with (3), the low-pass equivalent time-discrete signal for $n = 0, 1, \ldots, N-1$ becomes

$$s[n] = \frac{1}{\sqrt{M}} \sum_{k=0}^{M-1} X[\pi[k]] e^{j\frac{2\pi}{N}nk} \tag{4}$$

$$= \sum_{m=0}^{M-1} x[m] g[m, n] \tag{5}$$

where the basis function for symbol m is defined as

$$g[m, n] = \frac{1}{M} \sum_{k=0}^{M-1} e^{-j\frac{2\pi}{M}m\pi[k]} e^{j\frac{2\pi}{N}nk} \tag{6}$$

and N ($N \geq M$) is the number of subcarriers. A cyclic prefix (CP) of length N_{CP} is prepended to the signal for $n = -N_{\mathrm{CP}}, -N_{\mathrm{CP}}+1, \ldots, -1$. The allocated M subcarriers are assumed to be located contiguously, which is in accordance with the uplink frequency resource allocation in LTE/NR. The term N/M can be regarded as an oversampling factor. In the following analysis in Section II and for the evaluations of BER/BLER in Sections III-A and III-B, we will consider $N = M$ and return to the case of $N > M$ in Section III-C, where we consider the PAPR issue.

B. CHANNEL MODEL

We assume a time-discrete channel

$$h[n] = \sum_{l=0}^{L-1} \sqrt{\mathcal{P}_l} \tilde{h}_l[n] \delta[n - \tau_l] \tag{7}$$

with the relative channel tap power $\mathcal{P}_l$ and sample delay $\tau_l \ \forall l = 0, 1, \ldots, L-1$. A time-variant channel based on Clarke's two-dimensional isotropic scattering Rayleigh fading model [20] is used

$$\tilde{h}_l[n] = \frac{1}{\sqrt{P}} \sum_{p=1}^{P} e^{j(2\pi f_{\mathrm{D}} n \cos\theta_p + \phi_p)} \tag{8}$$

where P is the number of propagation paths per channel tap, f_{D} is the maximum Doppler frequency and θ_p and ϕ_p are the angle of arrival and initial phase of the pth propagation path, respectively. Both θ_p and ϕ_p are random variables uniformly distributed over $[-\pi, \pi)$ for all p and they are mutually independent.

C. RECEIVED SIGNAL

The received signal, $r[n]$, is obtained from convolution of $s[n]$ with $h[n]$, and by adding additive white Gaussian noise (AWGN), $\eta[n]$. Assuming that $N_{\mathrm{CP}} \geq \tau_{L-1}$, after removing the CP, $r[n]$ can be expressed as

$$r[n] = \sum_{l=0}^{L-1} \sqrt{\mathcal{P}_l} \tilde{h}_l[n] s[n - \tau_l \pmod N] + \eta[n] \tag{9}$$

$$= \sum_{m=0}^{M-1} x[m] \frac{1}{M} \sum_{k=0}^{M-1} \left(\sum_{l=0}^{L-1} \sqrt{\mathcal{P}_l} \tilde{h}_l[n] e^{-j\frac{2\pi}{N}\tau_l k} \right) \times e^{-j\frac{2\pi}{M}m\pi[k]} e^{j\frac{2\pi}{N}nk} + \eta[n] \tag{10}$$

where (5) and (6) were inserted in (9). By defining

$$H[n, k] = \sum_{l=0}^{L-1} \sqrt{\mathcal{P}_l} \tilde{h}_l[n] e^{-j\frac{2\pi}{N}\tau_l k} \tag{11}$$

$$D[v, k] = \frac{1}{\sqrt{N}} \sum_{n=0}^{N-1} H[n, k] e^{-j\frac{2\pi}{N}vn} \tag{12}$$

where (11) is the time-frequency channel transfer function and (12) is the Doppler-frequency channel transfer function, the received signal at subcarrier $c = 0, 1, \ldots, M-1$ is

$$R[c] = \frac{1}{\sqrt{N}} \sum_{n=0}^{N-1} r[n] e^{-j\frac{2\pi}{N}cn} \tag{13}$$

$$= \sum_{m=0}^{M-1} x[m] \frac{1}{M} \sum_{k=0}^{M-1} D[c-k, k] e^{-j\frac{2\pi}{M}m\pi[k]} + \tilde{\eta}[c] \tag{14}$$

$$= D[0, c] X[\pi[c]] + \sum_{\substack{k=0 \\ k \neq c}}^{M-1} D[c-k, k] X[\pi[k]] + \tilde{\eta}[c] \tag{15}$$

where $\tilde{\eta}[c] = 1/\sqrt{N} \sum_{n=0}^{N-1} \eta[n] e^{-j\frac{2\pi}{N}cn}$. From (10), we could identify the effective basis function subject to the channel as $\bar{g}[m, n] = \frac{1}{M} \sum_{k=0}^{M-1} H[n, k] e^{-j\frac{2\pi}{M}m\pi[k]} e^{j\frac{2\pi}{N}nk}$. From (15), it can be observed that the effect of the channel is a scaling and phase rotation factor ($D[0, c]$) and the sum which comprises inter-carrier interference (ICI) that may lead to an error floor.

D. LINEAR PERMUTATION POLYNOMIAL

An LPP is defined by $\pi[k] = f_1 k + f_0 \pmod M$ where $\gcd(f_1, M) = 1$ and f_0 is any integer. An interleaver based on an LPP results in a permuted DFT-s-OFDM signal, which is contained in the following property proven in Appendix A-A.

Property 1: With an LPP interleaver, $s[n]$ is a time-interleaved and phase modulated DFT-s-OFDM signal,

$$s[n] = x\left[n f_1^{-1} \pmod M \right] e^{-j\frac{2\pi}{M}nf_1^{-1}f_0} \tag{16}$$

where $f_1^{-1} f_1 \equiv 1 \pmod M$.

From the proof of Property 1, the basis function can be identified as

$$g[m, n] = e^{-j\frac{2\pi}{M}f_0 m} \delta\left[n - m f_1 \pmod M \right]. \tag{17}$$

Since (16) and (17) describe time division multiplexing (TDM) of the modulation symbols, it is not expected that an LPP will improve the BER/BLER compared to DFT-s-OFDM.

E. QUADRATIC PERMUTATION POLYNOMIAL

A QPP is defined by $\pi[k] = f_2k^2 + f_1k + f_0 \,(\mathrm{mod}\, M)$. Conditions on the f_2 and f_1 coefficients can be found in, e.g., [18], and f_0 is any integer. Let $M = p_0^{l_0}p_1^{l_1} \cdot \ldots \cdot p_r^{l_r}$ be the prime factorization of M where $p_i, i = 0, 1, \ldots, r$ are prime numbers and the multiplicities $l_i > 0$ are integers. Then, the conditions on the QPP coefficients can be succinctly stated as [21]:

i. If $p_i = 2, l_i = 1$ then $f_1 + f_2 \neq 0 \,(\mathrm{mod}\, 2)$.
ii. If $p_i = 2, l_i > 1$ then $f_1 \neq 0 \,(\mathrm{mod}\, 2)$ and $f_2 \equiv 0 \,(\mathrm{mod}\, 2)$.
iii. If $p_i > 2, l_i \geq 1$ then $f_1 \neq 0 \,(\mathrm{mod}\, p_i)$ and $f_2 \equiv 0 \,(\mathrm{mod}\, p_i)$.

QPP interleavers have been designed particularly for turbo codes, cf. [22], [23]. Such QPPs have been selected to facilitate implementations with parallel contention-free decoding and to achieve low error probability. However, in that context, the interleaver is internal and part of the error correcting code, and does not serve the purpose of a channel interleaver. Herein, the main objective is channel interleaving over time-frequency selective channels. Thus, the previous QPP interleavers are not directly relevant and new design criteria will be needed, which we address in Section III. With a QPP interleaver, the signal (4) with $N = M$ becomes,

$$s[n] = \frac{1}{M}\sum_{m=0}^{M-1} x[m]e^{-j\frac{2\pi}{M}f_0m}\sum_{k=0}^{M-1} e^{j\frac{2\pi}{M}k(n-mf_1-kmf_2)} \quad (18)$$

where the inner sum is a generalized quadratic Gauss sum.

Certain QPPs, i.e., irreducible QPPs, produce permutations which cannot equivalently be obtained from an LPP. It has been shown that a QPP is irreducible if and only if $M > \gcd(M, 2f_2)$ [22]. Moreover, two distinct QPPs could produce the same permutation. The number of irreducible QPPs which provide unique permutations depends on M and can be computed by given formulas [21], [24]. In [22], it was shown that if M is divisible by 8, there exists an irreducible QPP. More generally, according to [21], when the prime factorization of M is such that $p_0 = 2$, $l_0 = 0$, or 1, or 2 and $l_i = 1, i = 1, 2, \ldots, r$, then there exist no irreducible QPPs. Thus, such M should be excluded for the construction of QPPs. In LTE and NR, resources are allocated in multiples of resource blocks (RBs). The number of RBs is for the data channel using DFT-s-OFDM constrained to be $N_{\mathrm{RB}} = 2^{k_0}3^{k_1}5^{k_2}$ where k_0, k_1 and k_2 are non-negative integers [25]. A resource block contains $N_{\mathrm{sc}}^{\mathrm{RB}} = 12$ subcarriers, i.e., $M = N_{\mathrm{RB}}N_{\mathrm{sc}}^{\mathrm{RB}}$. Using the aforementioned conditions on M, it can be shown that the only resource allocations for which there would not exist an irreducible QPP are when $N_{\mathrm{RB}} = 1$ or $N_{\mathrm{RB}} = 5$, i.e., when $M = 12$ or $M = 60$.

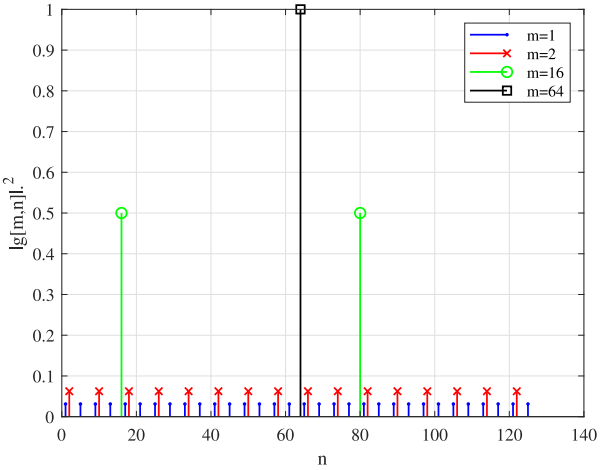

FIGURE 1. Example of $|g[m, n]|^2$ for $m = 1, 2, 16$ and 64 for $N = M = 128$ with $f[k] = 2k^2 + k$.

F. SIGNAL PROPERTIES OF INTERLEAVED DFT-S-OFDM

For the case of $N = M$, it is straightforward to verify that the basis function for DFT-s-OFDM is obtained with $f[k] = k$, and (6) simplifies to $g[m, n] = \delta[n-m]$. That is, modulation symbol $x[m]$ is transmitted on time sample m, which results in TDM of the symbols. The basis function is sparse since only 1 out of M samples is non-zero, i.e., carries a modulation symbol, and $M - 1$ samples are zeros. By using the geometric sum identity

$$\sum_{k=0}^{N-1} e^{j\frac{2\pi}{N}nk} = N\delta[n \,(\mathrm{mod}\, N)] \quad (19)$$

for any integer n, it can be shown from (6) that $g[0, n] = \delta[n]$ for any interleaver, i.e., it contains 1 non-zero sample. However, our evaluations of (6) with random permutations have shown that the basis functions for $m > 0$ are typically such that $g[m, n] \neq 0$. On the other hand, if a permutation polynomial is used, the basis functions could still contain many zeros. A sufficient but not a necessary condition for zero-valued samples is as follows, which is proven in Appendix A-B.

Property 2: If

$$\tilde{\pi}[k] = n_0k - m_0f[k] \,(\mathrm{mod}\, M) \quad (20)$$

is a permutation for $k = 0, 1, \ldots, M-1$, then $g[m_0, n_0] = 0$.

Thus, through $f[k]$, it is clear that the polynomial coefficients will determine the zero-valued samples. Fig. 1 shows examples of basis functions obtained from a QPP, where it can be observed that the number of non-zero elements differ among the basis functions and that the power is constant on the non-zero samples for a given basis function. Since a basis function can have multiple distinct peaks, the modulation symbols are not transmitted by TDM.

The basis functions can be further characterized by the periodic crosscorrelation function (PCCF), according to the following property which is proven in Appendix A-C.

Property 3: The PCCF of basis functions is

$$\rho_{g_m g_p}[d] = \sum_{n=0}^{M-1} g[m,n] g^*\big[p, n+d \,(\mathrm{mod}\, M)\big] \quad (21)$$

$$= g^*\big[p-m, d\big]. \quad (22)$$

Using (6), (19) and (22), it can be shown that

$$\rho_{g_m g_p}[0] = \delta[m-p] \quad (23)$$

and

$$\rho_{g_m g_m}[d] = \delta[d]. \quad (24)$$

Thus, according to (23) the basis functions are orthogonal, which simplifies a receiver and basic channel equalization methods could be applied. Furthermore, according to (24) a basis function has an ideal periodic autocorrelation function (PACF), i.e., it is orthogonal to any time delayed version of itself.

If $\{x[m]\}$ is a pre-defined sequence of symbols, the signal may be used for channel estimation, synchronization etc. In such cases the PACF of the signal becomes important, which is defined by

$$\rho_{ss}[d] = \sum_{n=0}^{M-1} s[n] s^*[n+d \,(\mathrm{mod}\, M)] \quad (25)$$

and the PACF for two modulation symbol sequences is

$$\rho_{xx}[d] = \sum_{n=0}^{M-1} x[n] x^*[n+d \,(\mathrm{mod}\, M)]. \quad (26)$$

The relation between the PACF of the signal and the basis functions (i.e., implicitly the interleaver) is given by the following property, which is proven in Appendix A-D.

Property 4: The PACF of the signal is

$$\rho_{ss}[d] = \sum_{n=0}^{M-1} \rho_{xx}[n] g^*[n,d]. \quad (27)$$

By utilizing Property 3 with $p = m+n$, we have for any m that $g^*[n,d] = \rho_{g_m g_{m+n}}[d]$, which could be inserted in to (27) to give the relation between the correlation functions of the signal, the modulation sequence and the basis functions. If the sequence $\{x[m]\}$ has ideal PACF, i.e., $\rho_{xx}[d] = \delta[d]$, then by using (6) and (19) in (27), it follows that $\rho_{ss}[d] = \delta[d]$. Hence, the ideal PACF property of $\{x[m]\}$ is invariant under frequency domain interleaving, which simplifies the construction of a reference symbol sequence and any suitable interleaver could be chosen.

Frequency domain interleaving does not change the power of the signal since the modulus sum of the basis functions in either time-domain or over basis functions is constant according to the following property, which is proven in Appendix A-E. Thus, for the purpose to select a permutation polynomial which reduces the PAPR, it suffices to select one to reduce the peak power of the signal.

Property 5: The power of the basis functions fulfill the following:

$$\left|\sum_{n=0}^{M-1} g[m,n]\right| = \left|\sum_{m=0}^{M-1} g[m,n]\right| = 1 \quad (28)$$

$$\sum_{n=0}^{M-1} |g[m,n]|^2 = \sum_{m=0}^{M-1} |g[m,n]|^2 = 1 \quad (29)$$

It should be pointed out that Property 2-5 were proven without the assumption that the interleaver is based a permutation polynomial. Hence, they apply for any type of permutation $\pi[k]$, including random interleaving. In the following, particular aspects of signal design using LPPs and QPPs will be considered.

III. SELECTION OF PERMUTATION POLYNOMIALS

A. QPP FOR REDUCING BER/BLER

The basis function (6) for DFT-s-OFDM with oversampling factor N/M becomes a sinc-like function (cf. (37) with $f_1 = 1$ and $f_0 = 0$), i.e., its power $|g[m,n]|^2$ has a single distinct peak which is located at sample $n = mN/M$, if N/M is an integer. We anticipate that better performance may be achieved on a time-varying channel for basis functions having multiple peaks, since the transmission of the modulation symbol then experiences diversity. For the case $N = M$, according to Property 2, the basis functions can have different number of non-zero elements and these can be regarded as the distinct peaks, cf. Fig. 1. In order to obtain basis functions having multiple distinct peaks, we therefore determine permutation polynomials that maximize the number of non-zero elements in the basis functions when $N = M$. Utilizing the unit step function $u(x)$, the novel criterion we propose to determine such polynomials is to select the QPP to maximize the number of non-zero elements over all M time-samples and M basis functions according to the function

$$V = \sum_{m=0}^{M-1} \sum_{n=0}^{M-1} u\Big(|g[m,n]|^2\Big). \quad (30)$$

The inner sum in (30) is the number of non-zero samples of a basis function, i.e., the number of distinct peaks of (6) when $N = M$. In Appendix A-J, the following is derived for a QPP

$$|g[m,n]|^2 = \frac{1}{M} \sum_{t=0}^{M-1} e^{-j\frac{2\pi}{M}(mf_2t^2 + (mf_1 - n)t}\, \delta[2mf_2 t \,(\mathrm{mod}\, M)] \quad (31)$$

which can be used to compute (30). Since a basis function has from 1 to M non-zero values, it is clear that the value range is $M \le V \le M^2$. In particular the lower limit applies to LPPs, according to the following property which is proven in Appendix A-F.

Property 6: If $\pi[k]$ is an LPP, then $V = M$.

Moreover, an upper bound of (30) can be found, according to the following property which is proven in Appendix A-G.

Property 7: If $\pi[k]$ is a QPP and M is even, then $V \le (M-1)M/2 + 1$.

TABLE 1. Example of QPPs and the number of non-zero values V for $M = 128$ and $M = 108$.

QPP ($M = 128$)	V	QPP ($M = 108$)	V
$f[k] = 2k^2 + k$	2732	$f[k] = 6k^2 + k$	732
$f[k] = 4k^2 + k$	1368	$f[k] = 18k^2 + k$	252
$f[k] = 8k^2 + k$	688	$f[k] = 54k^2 + k$	108
$f[k] = 16k^2 + k$	352	-	-
$f[k] = 32k^2 + k$	192	-	-
$f[k] = 64k^2 + k$	128	-	-

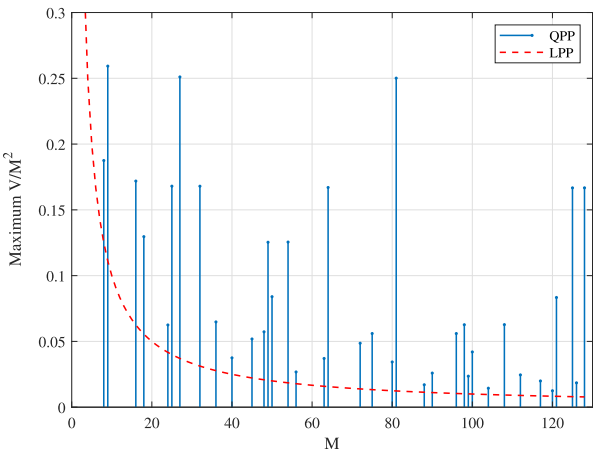

FIGURE 2. Maximum value of V/M^2 for irreducible QPPs and LPPs as function of M.

From Property 7, it follows that for QPPs with even M, $V/M^2 \leq 0.5$. The values of V contained in Table 1 are obtained by evaluating all QPPs for $M = 128$ and $M = 108$. It should be noted that there exist multiple QPPs for each value of V but only one is included in the table. In total 4032 and 612 unique QPPs were found for $M = 128$ and $M = 108$, respectively.

It can be seen that when $f_2 = M/2$, then $V = M$, i.e., the same value as for DFT-s-OFDM. That is the case where the signal becomes on the form (16), i.e., a permuted DFT-s-OFDM signal where a basis function is non-zero only on one sample, as shown by Property 6. This is because the condition $M > \gcd(2f_2, M)$ does not hold when $f_2 = M/2$ and those QPPs are reducible to an LPP, e.g., $64k^2 + k \equiv 65k \pmod{128}$.

For easier comparison of V values between different M, we consider the normalized value V/M^2, which by definition gives $V/M^2 \leq 1$. In Fig. 2, the maximum V/M^2 of a QPP is plotted for each feasible M, showing that the largest values of V/M^2 are achieved in particular when $M = 3^k$ and $M = 2^k$. Thus, the values of M for which there are QPPs with large V, are when the prime factorization of M is having a large multiplicity of one term p_i, i.e., its l_i large. The figure also contains the curve of $1/M$, which is the corresponding value of V/M^2 for an LPP.

In order to determine the QPPs which maximize the value V, the following sufficient condition for zero values of a basis function is useful, which is proven in Appendix A-H.

Property 8: If $\gcd(f_2, M) > 1$ and $\gcd(m_0 f_2, M) \nmid m_0 f_1 - n_0$, then $g[m_0, n_0] = 0$.

TABLE 2. Parameters for simulations of BER/BLER.

Parameter	Value
Number of symbols	$M = 128$
Number of subcarriers	$N = 128$
Channel	Vehicular A, 0 - 500 km/h Sum of $P = 20$ sinusoids/tap using [20]
Subcarrier spacing	$f_{\mathrm{SCS}} = 15$ kHz
Carrier frequency	$f_c = 6$ GHz
Receiver	MMSE (Appendix B)
Channel coding	Polar code, rate 1/3 and 3/4 with interleaving and rate matching according to [26]
Decoder	Successive cancellation list polar decoder [27]
Channel estimation	Ideal

This property implies that in order for basis function m to contain few zero samples, f_2 should be chosen such that

$$v = (mf_1 - n)/\gcd(mf_2, M) \tag{32}$$

becomes an integer for as many time samples n as possible. That is facilitated by minimizing the denominator of v. Moreover, the term mf_1 in (32) will, for a given m and f_2, not impact the number of instances where v is an integer. Thus, QPPs which maximize (30) could be confined to the QPPs minimizing $\gcd(f_2, M)$. Hence, a QPP which maximizes V could be constructed to have the smallest feasible value of f_2 for the given M, and f_1 is any feasible value according to the conditions of the coefficients of a QPP. As predicted by Property 8, the values of V in Table 1 are in decreasing order of $\gcd(f_2, M)$. Moreover, it can be confirmed from the conditions on the QPP coefficients that $f_2 = 2$ and $f_2 = 6$ are the smallest values of f_2 that are feasible for a QPP, for $M = 128$ and $M = 108$, respectively.

We have also evaluated random interleaving (i.e., the set of values $\{0, 1, \ldots, M-1\}$ is randomly permuted) and found that typically $V/M^2 \approx 1$, and that V does not show large variations among random interleaving sequences. Condition (30) is thus applicable for selecting permutation polynomials but is not suitable for selection among random interleaving sequences. It also means that the basis functions with random interleaver are typically dense. However, the difference between QPPs and random interleaving not only relates to V but also the distribution of power among the samples. Since the basis functions are dense for random interleaving, the power is much lower per sample than for basis functions of a QPP interleaver. Moreover, as shown in Fig. 1, for a QPP the power is constant for the samples where the basis function is not zero. We have not observed constant power for basis functions obtained from random interleaving. Thus, the potential gain of the larger value V of random interleaving may become limited by the non-uniform power distribution among the samples of the basis function.

B. SIMULATION RESULTS FOR BER/BLER

Considering the time-varying channel and the non-linear basis functions, it does not appear analytically tractable to determine expressions of BER/BLER on closed-form and we

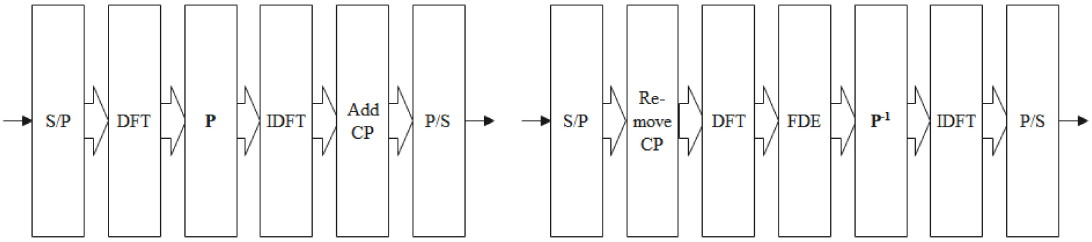

FIGURE 3. Block diagram of the DFT-s-OFDM transmitter, using an interleaver P, and the receiver using a deinterleaver $\mathbf{P}^{-1}$ and frequency domain equalization (FDE).

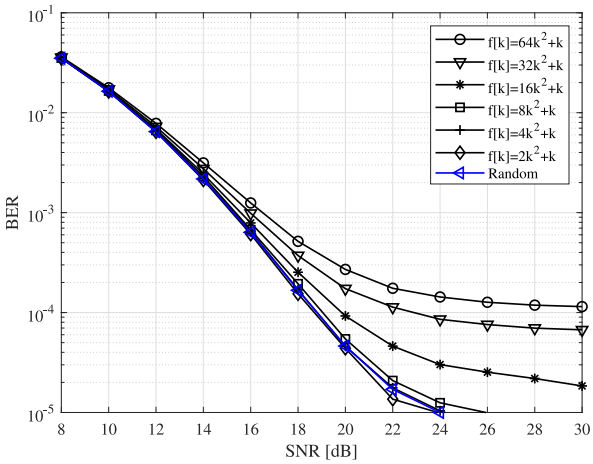

FIGURE 4. Bit error rate for QPSK as function of SNR for different QPPs on a Vehicular A channel with 500 km/h velocity for $M = 128$. The BER for random interleaving is also included.

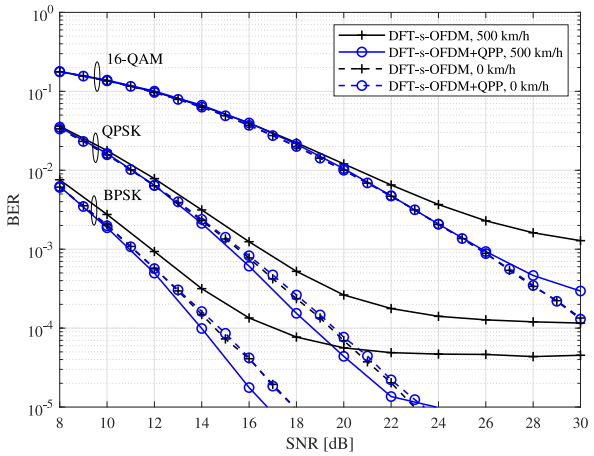

FIGURE 5. Bit error rate for BPSK, QPSK and 16-QAM as function of SNR for DFT-s-OFDM with and without QPP ($f[k] = 2k^2 + k$), on a Vehicular A channel with 0 km/h and 500 km/h velocity for $M = 128$.

use Monte-Carlo simulations according to the assumptions in Table 2 to compare performance with DFT-s-OFDM. A CP with $N_{\text{CP}} \geq \tau_{L-1}$ is attached to $s[n]$ and minimum mean square error (MMSE) frequency domain equalization (FDE) is used (see Appendix B). Ideal channel estimation is assumed, thus higher BER/BLER is expected in practice. Note that in [16], advanced iterative receivers were used, which may bring further gains. High speed scenarios for 5G have been defined up to 500 km/h [4] and we also evaluate 120 km/h and 350 km/h. We use a subcarrier spacing of $f_{\text{SCS}} = 15$ kHz and a carrier frequency of $f_c = 6$ GHz, which at 500 km/h corresponds to a maximum Doppler shift of 2.78 kHz, i.e., 19% of the subcarrier spacing. For BLER evaluation, the 3GPP NR polar code and rate matching is used [26] with a decoding algorithm according to [27]. In these simulations, the coded bits are mapped to modulation symbols which are transmitted in 1 DFT-s-OFDM symbol and the same permutation polynomial is used for all transmitted OFDM symbols. Fig. 3 gives a block diagram of the transmitter and receiver.

An issue at higher velocities is the existence of an error floor, which arises due to that the orthogonality among the subcarriers is not maintained, cf. (15). Fig. 4 shows uncoded BER as function of SNR for QPSK. It confirms that polynomial selection according to (30) works, since QPPs with a large V offer lower BER and suppress the error floor. A properly chosen QPP can result in better BER than for DFT-s-OFDM, which has the same BER as that of the reducible QPP $f[k] = 64k^2 + k$. The BER of random interleaving is also shown, i.e., a random interleaving sequence is generated for each transmission attempt and the BER is an average over the interleaver sequences. Thus the result can be interpreted as the expected BER for any random interleaving method. It can be concluded that the best QPP gives a BER comparable to random interleaving, despite that it has a value $V \ll M^2$. The selection of polynomial according to (30) is independent of modulation format, and Fig. 5 and Fig. 6 contain the BER for DFT-s-OFDM with the best QPP (i.e., $f[k] = 2k^2 + k$) which shows that the error floor can be suppressed significantly for the higher velocities, at least by an order of a magnitude for all the modulation formats. It can be seen that the relative gains of QPP interleaver increases with the velocity and for BPSK and QPSK, the BER decreases with the velocity when QPP is applied. For 16-QAM the diversity gain of QPP does not fully compensate for the loss due to the ICI, in comparison to the 0 km/h case. We apply the same condition (30) for determining a QPP for reducing the BLER, i.e., a QPP that maximizes the value V. The desired BLER depends on the application and typically ranges from 10^{-1} for mobile broadband (MBB) data to 10^{-5} for ultra reliable low-latency communication (URLLC) [28]. A channel code will be able to capture time-frequency diversity effects by itself. Nevertheless, Fig. 7 which contains the BLER with the same QPP as in Fig. 6,

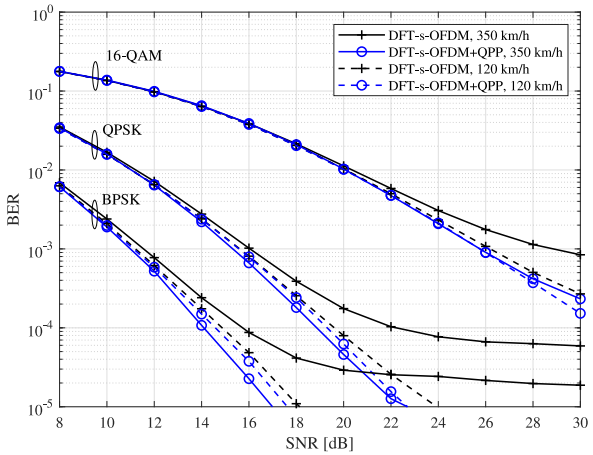

FIGURE 6. Bit error rate for BPSK, QPSK and 16-QAM as function of SNR for DFT-s-OFDM with and without QPP ($f[k] = 2k^2 + k$), on a Vehicular A channel with 120 km/h and 350 km/h velocity for $M = 128$.

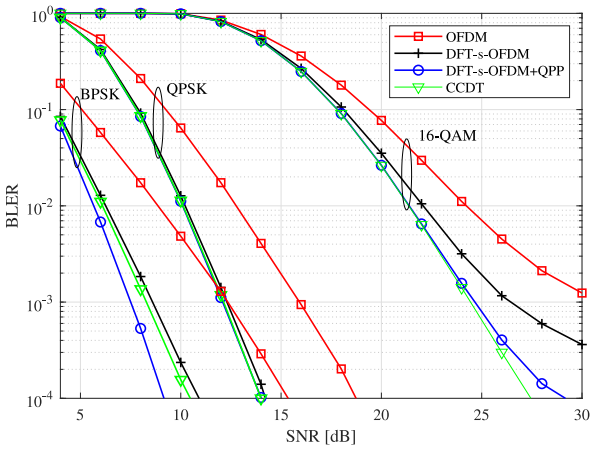

FIGURE 7. Block error rate for BPSK, QPSK and 16-QAM as function of SNR for DFT-s-OFDM with and without QPP ($f[k] = 2k^2 + k$), for OFDM and for CCDT (with chirp parameters $\alpha = -2.5$ and $\beta = -2$) on a Vehicular A channel with 500 km/h velocity for $M = 128$ with a polar code using code rate $r = 3/4$.

shows that there are substantial gains from QPP interleaving also with channel coding, especially for BPSK and for low BLER. It should be noted that this polar code is specified for QPSK in 3GPP NR system and we apply it herein also for BPSK and 16-QAM. As a further performance reference, OFDM is included, which is shown to provide larger BLER than the DFT-s-OFDM based schemes. Moreover, results for the chirp-based waveform CCDT [8] are included, which is shown to also be better than for DFT-s-OFDM.

C. LPP FOR REDUCING PAPR

The power dynamics of the baseband signal can be characterized by the peak-to-mean envelope power ratio (PMEPR) [29]. The PMEPR should ideally be evaluated on the time-continuous signal but as an approximation, the oversampled signal can be used and we define

$$\text{PMEPR} = \max_{0\le n\le N-1} \frac{|s[n]|^2}{\frac{1}{N}\sum_{n=0}^{N-1}|s[n]|^2}. \tag{33}$$

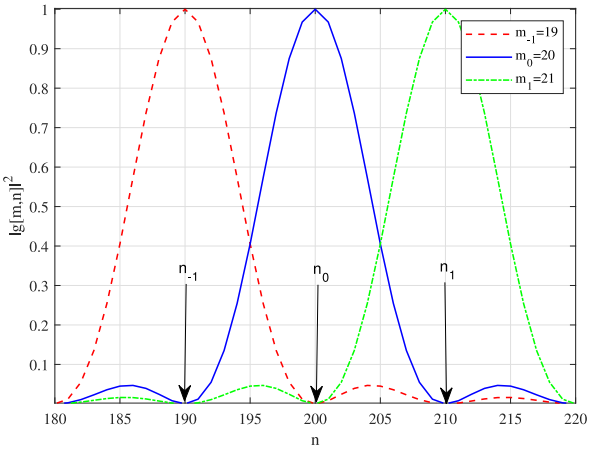

FIGURE 8. Example of $|g[m, n]|^2$ for different values of m with $N/M = 10$, $f_1 = 1$ and $f_0 = 0$.

If we consider an LPP and oversampling by a factor N/M, the signal can be expressed for $n = 0, 1, \ldots, N-1$ as

$$s[n] = \frac{1}{M}\sum_{m=0}^{M-1} x[m] \sum_{k=0}^{M-1} e^{-j\frac{2\pi}{M}m(f_1k+f_0)} e^{j\frac{2\pi}{N}nk} \tag{34}$$

$$= \frac{1}{M}\sum_{m=0}^{M-1} x[m] e^{-j\frac{2\pi}{M}mf_0} e^{j\pi\frac{M}{N}\left(n-\frac{N}{M}f_1m\right)\left(1-\frac{1}{M}\right)} \times \frac{\sin\left(\pi\frac{M}{N}\left(n-\frac{N}{M}f_1m\right)\right)}{\sin\left(\pi\frac{1}{N}\left(n-\frac{N}{M}f_1m\right)\right)} \tag{35}$$

$$= \sum_{m=0}^{M-1} x[m] \underbrace{e^{-j\frac{2\pi}{M}mf_0}\frac{1}{M}h\left[n-\frac{N}{M}f_1m\right]}_{g[m,n]} \tag{36}$$

with the Dirichlet kernel

$$h[k] = e^{j\pi\frac{M}{N}k\left(1-\frac{1}{M}\right)} \frac{\sin\left(\pi\frac{M}{N}k\right)}{\sin\left(\pi\frac{1}{N}k\right)}. \tag{37}$$

Thus, (36) and (37) show that the signal can be expressed by a set of basis functions, $g[m, n]$, which are non-linear in the LPP coefficients. According to Property 5, the interleaver does not change the average transmitted power of the signal, thus minimization of the PMEPR reduces to minimizing $|s[n]|^2$. As opposed to (16), where $N = M$ and the PMEPR does not depend on the interleaver, the LPP coefficients in the basis functions for (37) could affect the PMEPR.

Fig. 8 shows an example of the power of basis function $|g[m, n]|^2$ for a limited set of values n, and for $m = 19, 20, 21$, where it is assumed that $f_1 = 1$, $f_0 = 0$ and $N/M = 10$. It can be seen that symbol m_0 is modulated on basis function $g[m_0, n]$ which has its main power peak $|g[m_0, n_0]|^2$ at sample $n_0 = N/Mm_0$. Likewise, the basis function for symbol m_1 will have its power peak at sample $n_1 = N/Mm_1$. Fig. 8 illustrates that the signal power contribution on samples $n_0 < n < n_1$, where $n_1 = N/Mm_1 = N/Mm_0 + N/M$ and $m_1 = m_0 + 1$, and $n_{-1} = N/Mm_{-1}$ and $m_{-1} = m_0 - 1$, are from symbol m_{-1}, m_0 and m_1. However, the main power contribution is from m_0

and m_1, i.e., consecutive basis functions. The basis function in (36) and (37) contains a phase term and an amplitude term and it can be found that the phase term for modulation symbol m in $g[m, n]$ for time samples between the peaks of two consecutive basis functions is,

$$\theta(m) = e^{-j\frac{2\pi}{M}mf_0} e^{-j\pi f_1 m\left(1-\frac{1}{M}\right)} \tag{38}$$

$$= e^{-j\frac{2\pi}{M}m\left(f_0-\frac{f_1}{2}\right)} e^{-j\pi m f_1} \tag{39}$$

where the phase term being dependent on the time sample n in (36), which is common to all basis functions m, has been removed. Thus, the phase difference between basis functions for two consecutive modulation symbols m_0 and $m_1 = m_0 + 1$ is

$$\arg\big(\theta(m_0)\theta^*(m_0+1)\big) = \frac{2\pi}{M}\left(f_0 - \frac{f_1}{2}\right) + \pi f_1. \tag{40}$$

To reduce the peak power on samples $n_0 < n < n_1$, different phase values should be used for symbol m_0 and m_1, such that their basis functions do not add coherently. Therefore, f_0 and f_1 should be chosen to rotate the modulation symbol constellation such that for any consecutive symbols $x[m_0]$ and $x[m_1]$ taken from the modulation constellation, it holds that

$$x[m_0]\theta(m_0) \neq x[m_1]\theta(m_1). \tag{41}$$

We propose that this could be achieved by rotating the constellation an angle according to (40) as,

$$\frac{2\pi}{M}\left(f_0 - \frac{f_1}{2}\right) + \pi f_1 \approx \frac{\pi t}{4}(2q+1) \tag{42}$$

where $t = 1$ for QPSK and 16-QAM, $t = 2$ for BPSK and q is an integer. Consider first the case $f_1 = 1$ where q is chosen such that f_0 is a positive integer. From (42) we can solve for f_0, and it follows that

$$f_0 = \left\lfloor \frac{M}{2}\left(\frac{t(2q+1)}{4} - 1\right) + \frac{1}{2} \right\rfloor \tag{43}$$

or

$$f_0 = \left\lceil \frac{M}{2}\left(\frac{t(2q+1)}{4} - 1\right) + \frac{1}{2} \right\rceil. \tag{44}$$

The resulting phase rotations of (43) or (44) may not be the optimal ones since, firstly, they are derived based on the assumed phase angle of (42) which may not be optimal and, secondly, because the desired phase angle may not be achieved perfectly since f_0 and f_1 have to be integer coefficients of an LPP. The results in Fig. 9, where the 1-percentile of the complementary cumulative distribution function (CCDF) of the PMEPR, which is obtained from simulations, is plotted as function of f_0, confirm that (43) and (44) reduce the PMEPR for QPSK and 16-QAM. The PMEPR becomes periodic in f_0 since (39) is periodic. The PMEPR reduction is moderate, i.e., fractions of a dB, for QPSK and 16-QAM. A comparison is also made to BPSK and $\pi/2$-BPSK, where the gains are substantial, i.e., several dB. It can be seen that the PMEPR curve for BPSK is a cyclically shifted version of the $\pi/2$-BPSK PMEPR curve.

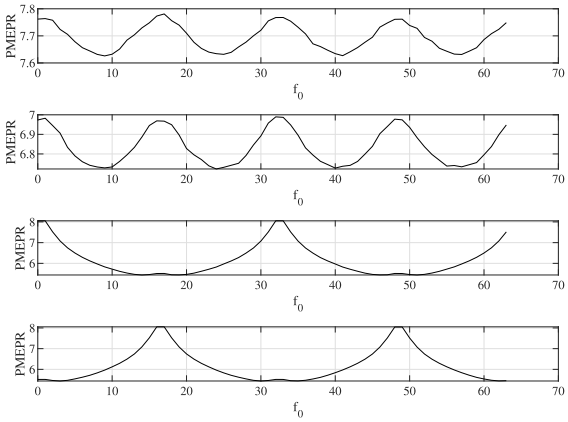

FIGURE 9. PMEPR [dB] at 1-percentile CCDF as function of f_0 for $f_1 = 1$, for 16-QAM (top), QPSK, BPSK and $\pi/2$-BPSK (bottom). Oversampling by a factor $N/M = 10$ is used and $M = 64$.

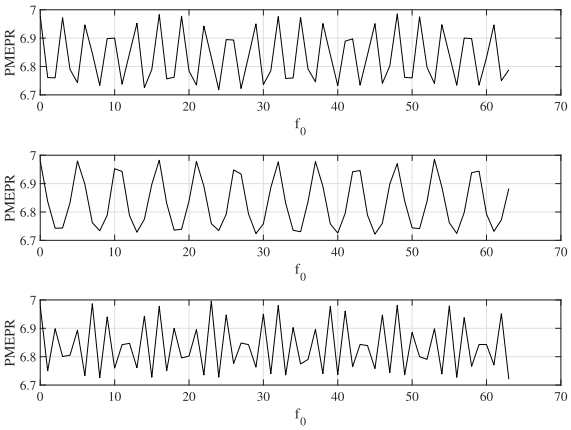

FIGURE 10. PMEPR [dB] at 1-percentile CCDF as function of f_0 for $f_1 = 3$ (top), $f_1 = 5$ (middle) and $f_1 = 7$ (bottom), for QPSK. Oversampling by a factor $N/M = 10$ is used and $M = 64$.

The lowest PMEPR for BPSK is obtained with $f_0 = 14$, which corresponds to the effective rotation angle $27\pi/64$, i.e., slightly less than $\pi/2$. Notably, phase rotation angles in the vicinity of $\pi/2$ have been identified to minimize the PMEPR for BPSK in [30].

For the case $f_1 \neq 1$, it follows from (36) and (37) that $|g[m_0, n_0]|^2$ has its main peak at sample $n_0 = N/Mf_1m_0 \,(\mathrm{mod}\, N)$ and for m_1, the main peak is at sample $n_1 = N/Mf_1m_1 \,(\mathrm{mod}\, N)$. Therefore, it may be that the main power contribution on samples $N/Mf_1m_0 < n < N/Mf_1m_0 + N/M$ does not come from a modulation symbol being consecutive to m_0, i.e., if $N/Mf_1m_1 \,(\mathrm{mod}\, N) \neq N/Mf_1m_0 + N/M$. Therefore, $\arg(\theta(m_0)\theta^*(m_0+1))$ can depend on the symbol index m_0 which makes it difficult to analytically derive a proper value of f_0. However, as shown in Fig. 10, there is a periodicity in the PMEPR and some values of f_0 are better than others, but there is no significant gain compared to when $f_1 = 1$ as in Fig. 9. Fig. 11 contains the CCDF of the PMEPR for an LPP according to (43) and for DFT-s-OFDM (i.e., $f[k] = k$). The PMEPR reduction is significant for BPSK, while being moderate for QPSK and 16-QAM.

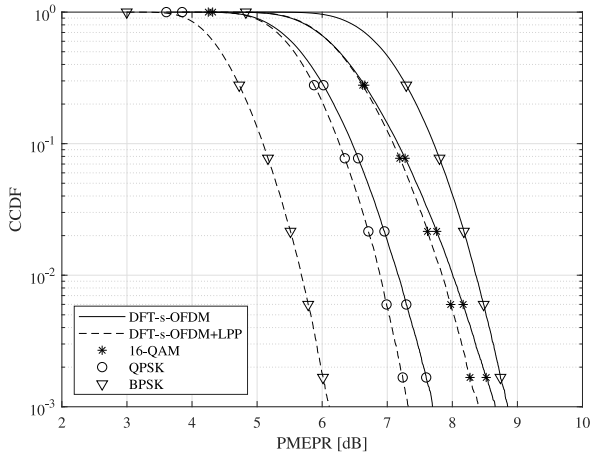

FIGURE 11. CCDF of PMEPR for BPSK, QPSK and 16-QAM for DFT-s-OFDM with and without LPP. Oversampling by a factor $N/M = 10$ is used and $M = 128$.

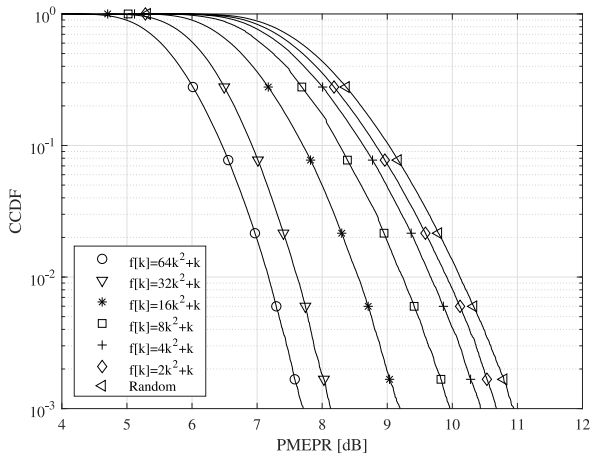

FIGURE 12. CCDF of PMEPR for QPSK using the QPPs from Table 1 and random interleaving. Oversampling by a factor $N/M = 10$ is used and $M = 128$.

D. RELATION BETWEEN PMEPR AND BER/BLER

A basis function with QPP interleaver may not be a sinc-like function and can have multiple peaks (in contrast to the distinct single peak of the LPP basis function (37) shown in Fig. 8), and it may also not have a symmetric shape. Therefore, it is not straightforward to analytically determine the best QPP coefficients in order to reduce the PMEPR, as could be done for an LPP. Fig. 12 contains simulation results of the CCDF for the PMEPR for QPSK using the QPPs of Table 1 and for random interleaving, which is shown to produce the largest PMEPR. Comparing with Fig. 4, it can be concluded that the QPPs which offer the lowest PMEPR give the highest BER.

The results in Fig. 4 and Fig. 12 suggest that either the PMEPR or the BER/BLER is improved. To investigate this further, we set $M = 32$, which makes it feasible to perform a complete exhaustive search. That is, we generate all LPPs and all irreducible QPPs and for each one of them, signals are produced and simulations are made to determine the PMEPR at the 1-percentile of the CCDF. Then we select the polynomial which minimizes the PMEPR and the uncoded BER is evaluated by simulations for this polynomial to determine the required SNR to achieve 10^{-2} BER. These results are contained in Table 3 and Table 5, which show that LPP reduces the PMEPR, especially for BPSK, but not the BER. However, we note that for BPSK, there exist QPPs (e.g., $f[k] = 8k^2 + 7k + 4$) which simultaneously reduce the PMEPR and the BER, compared to DFT-s-OFDM. The SNR gain of random interleaving is not significant compared to QPP, which also has much lower PMEPR. Table 4 contains the required SNR to achieve 10^{-3} BLER, assuming the best QPP from Table 1 which minimizes the BLER and the LPP is selected to minimize the PMEPR according to (43). It can be seen that the QPP improves the BLER more for the higher code rate and the gains are larger for BPSK and 16-QAM. The LPP improves the PMEPR more for BPSK than for QPSK and 16-QAM. Random interleaving has no significant gain over a QPP interleaver.

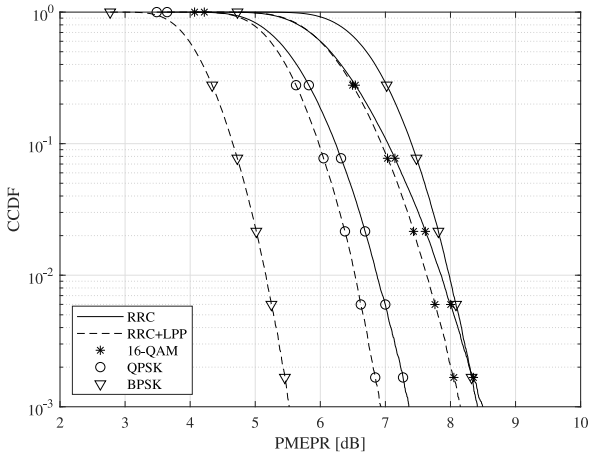

FIGURE 13. CCDF of PMEPR for BPSK, QPSK and 16-QAM using an LPP and FDSS with RRC window with roll off factor 0.2. Oversampling by a factor $N/M = 10$ is used and $M = 128$.

E. LPP WITH FDSS

The PMEPR reduction methods of LPP and FDSS could be performed jointly such that the transmitted signal becomes

$$s[n] = \frac{1}{\sqrt{M}} \sum_{k=0}^{M-1} F[k]X[\pi[k]]e^{j\frac{2\pi}{N}nk} \tag{45}$$

where $F[k]$ is the FDSS window. For Fig. 13, a root raised cosine (RRC) window with roll off factor 0.2 has been used and the results show that the gains of the LPP method is maintained, and are specifically substantial for BPSK modulation.

IV. TRANSCEIVER ASPECTS

A frequency domain interleaver could be introduced for DFT-s-OFDM with small impact. Nevertheless, a few options for the implementation are discussed in this section.

TABLE 3. PMEPR [dB] at the 1-percentile CCDF and required SNR [dB] for BER = 10^{-3} for polynomials found through exhaustive search that minimize the PMEPR for DFT-s-OFDM with and without LPP. Oversampling by a factor $N/M = 10$ is used when evaluating the PMEPR and $M = 32$.

	BPSK		QPSK		16-QAM	
	PMEPR	SNR	PMEPR	SNR	PMEPR	SNR
DFT-s-OFDM	7.62	6.81	6.77	10.6	7.54	20.1
LPP	5.21	6.82	6.49	10.6	7.29	20.1
QPP	6.11	6.21	7.12	10.4	7.56	19.9
Random	9.13	6.27	9.15	10.1	9.13	19.7

TABLE 4. PMEPR [dB] at the 1-percentile CCDF and required SNR [dB] for BLER = 10^{-3} for code rate $r = 3/4$ and $r = 1/3$, for DFT-s-OFDM with and without LPP and QPP. Oversampling by a factor $N/M = 10$ is used when evaluating the PMEPR and $M = 128$.

	BPSK			QPSK			16-QAM		
	PMEPR	SNR ($r = 1/3$)	SNR ($r = 3/4$)	PMEPR	SNR ($r = 1/3$)	SNR ($r = 3/4$)	PMEPR	SNR ($r = 1/3$)	SNR ($r = 3/4$)
DFT-s-OFDM	8.4	0.7	8.6	7.2	3.9	12.3	8.0	17.2	26.5
LPP	5.7	0.7	8.6	6.9	3.9	12.3	7.9	17.2	26.5
QPP	10.1	0.1	7.5	9.9	4.0	12.1	9.9	17.3	24.7
Random	10.1	0	7.6	10.1	4.0	12.2	10.1	17.3	24.6

TABLE 5. Polynomials found through exhaustive search to minimize the 1-percentile CCDF of the PMEPR. Oversampling by a factor $N/M = 10$ is used and $M = 32$.

	LPP	QPP
BPSK	$f[k] = 25k + 31$	$f[k] = 8k^2 + 7k + 4$
QPSK	$f[k] = 5k + 17$	$f[k] = 8k^2 + 23k + 15$
16-QAM	$f[k] = 17k + 28$	$f[k] = 8k^2 + 21k + 19$

A. INVERSE PERMUTATION POLYNOMIALS

The receiver is performing the inverse operations of the transmitter, i.e., an N-point DFT, FDE, deinterleaving and an M-point inverse DFT (IDFT). Interleavers based on permutation polynomials allow for simple deinterleaving, which is applied on the received and equalized Fourier coefficients $Y[k]$ as $Y[\pi^{-1}[k]]$. The degree of $\pi^{-1}[k]$ may not be the same as for $\pi[k]$. The inverse permutation polynomial, and in particular minimum degree inverse permutation polynomials, could be determined by the algorithms in [18], [19], [22]. However, as will be shown, the inverse permutation polynomial $\pi^{-1}[k]$ always gives the same value $V_{\pi^{-1}}$ of (30) as for the associated permutation polynomial V_π. Thus it is not expected that there would be any significant difference in BER/BLER among them, which is captured by the following property proven in Appendix A-I.

Property 9: For a permutation polynomial $\pi[k]$ and its associated inverse permutation polynomial $\pi^{-1}[k]$,

$$V_{\pi^{-1}} = V_\pi. \tag{46}$$

A large degree of the permutation polynomial may increase the implementation complexity, which is more critical for the mobile terminal than for a base station. Thus, it would be possible to utilize the one permutation polynomial of $\pi[k]$ or $\pi^{-1}[k]$ which has the smallest degree in the mobile terminal.

B. COMPLEXITY REDUCTION OF QPP INTERLEAVER

Since M may be large, computing the values of (1) involves squaring and modulo operation of large integers. This could be avoided by decomposing the polynomial. In [31], it was shown that a QPP interleaver can be expressed as

$$\pi[k] = f_1 k + f_2 (k \bmod Q)^2 \bmod M) \tag{47}$$

where $Q\,(Q < M)$ depends on the prime factorization of M and of f_2. Hence, the number of squaring operations could be reduced from M to Q. Alternatively, complexity reductions can be made as follows. Suppose $f[k]$ is a QPP with $f_0 = 0$, then we have

$$f[k + d] = f[k] + f[d] + 2f_2 kd \tag{48}$$

and it is straightforward to verify that if

$$2f_2 kd \equiv 0 \,(\bmod M) \tag{49}$$

then, the permutation values can be computed by a linear relation

$$\pi[k + d] = \pi[k] + \pi[d] \,(\bmod M). \tag{50}$$

Thus, the number of permutation values which need to be computed by $\pi[k]$ can be reduced. One example fulfilling (49) is when $kd = M$. Furthermore, by letting $d = 1$ and recursively utilizing (48), we obtain for $k > 0$

$$f[k] = f[k - 1] + f_1 + f_2(2k - 1). \tag{51}$$

Moreover, by using the identity for the sum of natural numbers

$$\sum_{t=1}^{k-1} t = \frac{k(k-1)}{2} \tag{52}$$

an equivalent representation is

$$f[k] = (f_2 + f_1)k + f_2 k(k - 1) \tag{53}$$

$$= (f_2 + f_1)k + 2f_2 \sum_{t=1}^{k-1} t. \tag{54}$$

Hence, by utilizing either (51) or (54), squaring operations can be avoided in order to determine the permutation (1).

C. ALTERNATIVE SIGNAL GENERATION

An alternative representation of frequency interleaved DFT-s-OFDM is precoded DFT-s-OFDM, which is derived as follows. Define the matrices:

- DFT matrix: $\mathbf{W}_N = [w_{kl}]$ with $w_{kl} = 1/\sqrt{N}e^{-j\frac{2\pi}{N}kl}$ for $k, l = 0, 1, \ldots, N-1$.
- Mapping matrix: $\mathbf{Q} = [q_{kl}]$ with $q_{kl} \in \{0, 1\}$, $k = 0, 1, \ldots, N-1$ and $l = 0, 1, \ldots, M-1$, which maps a length-M vector to the set of $N (N \geq M)$ subcarriers.
- Permutation matrix: $\mathbf{P} = [p_{kl}]$ with $k = 0, 1, \ldots, M-1$ and $l = 0, 1, \ldots, M-1$, which for each k, $p_{kl} = 1$ if $l = \pi[k]$ and $p_{kl} = 0$ otherwise.
- Precoding matrix: $\mathbf{G} = \mathbf{W}_M^{\dagger}\mathbf{P}\mathbf{W}_M$

The signal vector $\mathbf{s} = [s[n]]'$ is obtained from the symbol vector $\mathbf{x} = [x[m]]'$ and since $\mathbf{W}_N^{\dagger}\mathbf{W}_N = \mathbf{W}_N\mathbf{W}_N^{\dagger} = \mathbf{I}$, an equivalent representation is given by

$$\mathbf{s} = \mathbf{W}_N^{\dagger}\mathbf{Q}\mathbf{P}\mathbf{W}_M\mathbf{x} \tag{55}$$

$$= \mathbf{W}_N^{\dagger}\mathbf{Q}\mathbf{W}_M\mathbf{G}\mathbf{x}. \tag{56}$$

Hence, from (56) it can be observed that frequency domain interleaving can alternatively be viewed as DFT-s-OFDM with a precoder $\mathbf{G}$ applied before the DFT precoder. Since $\mathbf{P}$ is an orthogonal matrix, it follows that the inverse precoder, e.g., to be used in the receiver, could be defined as $\mathbf{G}^{-1} = \mathbf{G}^{\dagger}$.

When $\mathbf{P}$ is derived from an LPP, the precoder $\mathbf{G}$ has simple structure. Namely, if $f_0 = 0$, then $\mathbf{G}$ is a permutation matrix. If $f_0 \neq 0$ and $N = M$, then $\mathbf{G}$ is a phase modulated permutation matrix. This could be realized as follows. Suppose $y[n]$ is the output from the precoder and that $q = f_1^{-1}$ is the inverse of f_1 modulo-M, which always exists since $\gcd(f_1, M) = 1$. Then, with $\mathbf{y} = [y[n]]'$ and $\mathbf{y} = \mathbf{G}\mathbf{x}$, it will hold that

$$y[n] = \frac{1}{\sqrt{M}}\sum_{m=0}^{M-1} X\big[f_1 m + f_0\big]e^{j\frac{2\pi}{M}mn} \tag{57}$$

$$= \frac{1}{\sqrt{M}}\sum_{m=0}^{M-1} X\big[f_1 m + f_0\big]e^{j\frac{2\pi}{M}(f_1 m + f_0)qn}e^{-j\frac{2\pi}{M}f_0 qn} \tag{58}$$

$$= \frac{e^{-j\frac{2\pi}{M}f_0 qn}}{\sqrt{M}}\sum_{k=0}^{M-1} X[k]e^{j\frac{2\pi}{M}kqn} \tag{59}$$

$$= e^{-j\frac{2\pi}{M}f_0 qn}x\big[qn \,(\mathrm{mod}\, M)\big]. \tag{60}$$

Hence, the $(n+1)$th row of $\mathbf{G}$ will contain $e^{-j\frac{2\pi}{M}f_0 qn}$ in column $qn \,(\mathrm{mod}\, M)+1$, and zeros otherwise. Generally, from the definition of $\mathbf{G} = [g_{kp}]$ for $k = 0, 1, \ldots, M-1$ and $p = 0, 1, \ldots, M-1$, it can be deduced that,

$$g_{kp} = \frac{1}{M}\sum_{n=0}^{M-1} e^{j\frac{2\pi}{M}nk}e^{-j\frac{2\pi}{M}\pi[n]p}$$

$$= g\big[p, k\big] \tag{61}$$

where the second step follows from (6). It is straightforward to verify that $g_{00} = 1$, $g_{0p} = 0, \forall p \neq 0$ and $g_{k0} = 0, \forall k \neq 0$ for an LPP with $f_0 = 0$, i.e., $\mathbf{G}$ is a permutation matrix. For a QPP, determining $\mathbf{G}$ involves evaluation of the generalized quadratic Gauss sum in (61), for which there are closed-form expressions only in some cases.

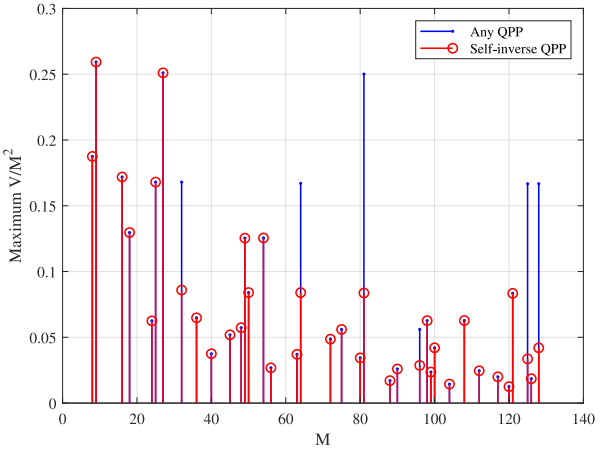

FIGURE 14. Maximum value of V normalized by M^2 for irreducible QPPs as function of M. The blue bars (dot) show the maximum value for any irreducible QPP, while the red bars (circle) are limited to only those irreducible QPPs which are self-inverses.

D. INVOLUTORY PERMUTATION POLYNOMIALS

A permutation matrix is involutory if $\mathbf{P}^2 = \mathbf{I}$, i.e., its inverse is the matrix itself. This means that the same permutation polynomial can be used for deinterleaving and for interleaving, i.e., the inverse permutation polynomial is the same as the permutation polynomial. In that case, the same interleaver can be used for transmission and reception, which reduces the implementation complexity. This requires that the self-inverse property holds

$$f[f[k]] \equiv k \,(\mathrm{mod}\, M) \tag{62}$$

and inserting a QPP into (62), the following congruence equations determine the necessary conditions.

$$f_2^3 \equiv 0 \,(\mathrm{mod}\, M) \tag{63}$$

$$2f_2^2 f_1 \equiv 0 \,(\mathrm{mod}\, M) \tag{64}$$

$$f_2 f_1^2 + 2f_2^2 f_0 + f_2 f_1 \equiv 0 \,(\mathrm{mod}\, M) \tag{65}$$

$$2f_2 f_1 f_0 + f_1^2 \equiv 1 \,(\mathrm{mod}\, M) \tag{66}$$

$$f_2 f_0^2 + f_1 f_0 + f_0 \equiv 0 \,(\mathrm{mod}\, M) \tag{67}$$

For example, it can be verified that $f[k] = 8k^2 + 63k$ is irreducible and fulfills (62) for $M = 128$. The results contained in Fig. 14 show that in most cases, a QPP which is its own self-inverse, has the same maximum value V as any other QPP for a given M.

It is also possible to construct LPPs which have the self-inverse property and the conditions are given by (63)–(67) with $f_2 = 0$. For example, for even M such an LPP is $f_1 = 1$ and $f_0 = M/2$. It has been shown that $\mathbf{P}$ commutes with the DFT matrix [32], i.e., $\mathbf{W}_M\mathbf{P} = \mathbf{P}\mathbf{W}_M$, if $\mathbf{P}$ is involutory and if it is derived from a permutation fulfilling $f[k] = f[1]k \,(\mathrm{mod}\, M)$ and $f[1]^2 \equiv 1 \,(\mathrm{mod}\, M)$. Thus, such a permutation could be generated from an LPP with $f_1^2 \equiv 1 \,(\mathrm{mod}\, M)$ and $f_0 = 0$, which satisfy (63)–(67). If $\mathbf{P}$ commutes with $\mathbf{W}_M$, the basis functions become very simple,

since $\mathbf{G} = \mathbf{P}$. The number of solutions to $f_1^2 \equiv 1 \,(\mathrm{mod}\, M)$ depends on M. However, there are at least two solutions, i.e., $f_1 = 1$ and $f_1 = M - 1$. To summarize, there exist plenty of self-inverse QPPs which maximize V. However, self-inverse LPPs do not typically fulfill any of the PMEPR minimizing conditions (43)–(44).

V. CONCLUSION

Frequency-domain interleaving could be straightforwardly introduced in existing 4G/5G systems utilizing DFT-s-OFDM, without significant changes to the transmit/receive chain implementation. The interleaver will also not impact the spectrum of the transmitted signal, e.g., out-of-band emissions. The proposed novel criteria for constructing permutation polynomials result in improved BER/BLER on channels with high Doppler spread and can produce lower PAPR than for DFT-s-OFDM. Notably, for some cases, e.g., BPSK with QPP, both the BER/BLER and PAPR can be improved simultaneously. Random interleaving provides much worse PAPR and has no obvious advantage, in terms of performance or implementation complexity. With a QPP interleaver the basis functions have different shapes, e.g., different number of peaks, which suggests that modulation symbols carried on different basis functions may experience unequal reliability. We leave for further study the construction of permutation polynomials considering this aspect as well as use of cubic permutation polynomials. Moreover, the case of discontiguously located subcarriers, evaluation with advanced receivers and channel estimation could be considered.

APPENDIX A

A. PROOF OF PROPERTY 1

$$\begin{aligned} s[n] &= \frac{1}{M}\sum_{m=0}^{M-1} x[m] \sum_{k=0}^{M-1} e^{-j\frac{2\pi}{M}m\pi[k]} e^{j\frac{2\pi}{M}nk} \\ &= \frac{1}{M}\sum_{m=0}^{M-1} x[m] \sum_{k=0}^{M-1} e^{-j\frac{2\pi}{M}m(f_1k+f_0)} e^{j\frac{2\pi}{M}nk} \\ &= \frac{1}{M}\sum_{m=0}^{M-1} x[m] e^{-j\frac{2\pi}{M}f_0m} \sum_{k=0}^{M-1} e^{j\frac{2\pi}{M}k(n-mf_1)} \\ &= x\Big[nf_1^{-1} \,(\mathrm{mod}\, M)\Big] e^{-j\frac{2\pi}{M}nf_1^{-1}f_0} \end{aligned} \tag{68}$$

In the last step, the inner sum exists only when the linear congruence equation $mf_1 \equiv n \,(\mathrm{mod}\, M)$ has a solution. It is known that a solution exists if $n \equiv 0 \,(\mathrm{mod}\, \gcd(f_1, M))$. Since $\pi[k]$ is a permutation polynomial, $\gcd(f_1, M) = 1$, therefore there exists a unique $m = nf_1^{-1}$ for every n, where $f_1^{-1}f_1 \equiv 1 \,(\mathrm{mod}\, M)$.

B. PROOF OF PROPERTY 2

A sufficient condition for the sum $g[m_0, n_0] = \frac{1}{M}\sum_{k=0}^{M-1} e^{-j\frac{2\pi}{M}m_0\pi[k]} e^{j\frac{2\pi}{M}n_0k}$ to vanish is that $n_0k - m_0\pi[k]$ generates a set of values $\{q, q+1, \ldots, q+M-1\}$ for any integer q. This occurs if $\tilde{\pi}[k] = n_0k - m_0f[k] \,(\mathrm{mod}\, M)$ is a permutation. The sum could also vanish for other sets of values, therefore the condition is sufficient but not necessary.

C. PROOF OF PROPERTY 3

$$\begin{aligned} \rho_{g_mg_p}[d] &= \frac{1}{M^2}\sum_{k=0}^{M-1}\sum_{r=0}^{M-1} e^{j\frac{2\pi}{M}(p\pi[r]-m\pi[k])} e^{-j\frac{2\pi}{M}dr} \\ &\quad \times \sum_{n=0}^{M-1} e^{j\frac{2\pi}{M}n(k-r)} \\ &= \frac{1}{M}\sum_{r=0}^{M-1} e^{j\frac{2\pi}{M}(p-m)\pi[r]} e^{-j\frac{2\pi}{M}dr} \\ &= g^*\big[p-m, d\big] \end{aligned} \tag{69}$$

D. PROOF OF PROPERTY 4

Using Property 3, it follows that

$$\begin{aligned} \rho_{ss}[d] &= \sum_{n=0}^{M-1}\sum_{m=0}^{M-1}\sum_{p=0}^{M-1} x[m]\ g[m,n]x^*[p]\ g^*\big[p, n+d\big] \\ &= \sum_{m=0}^{M-1}\sum_{p=0}^{M-1} x[m]\ x^*[p] \sum_{n=0}^{M-1} g[m,n]g^*\big[p, n+d\big] \\ &= \sum_{m=0}^{M-1}\sum_{p=0}^{M-1} x[m]\ x^*[p]\ \rho_{g_mg_p}[d] \\ &= \sum_{m=0}^{M-1}\sum_{p=0}^{M-1} x[m]\ x^*[p]\ g^*\big[p-m \,(\mathrm{mod}\, M), d\big] \\ &= \sum_{m=0}^{M-1}\sum_{t=0}^{M-1} x[m]\ x^*[m+t]g^*[t,d] \\ &= \sum_{t=0}^{M-1} \rho_{xx}[t]\ g^*[t,d] \end{aligned} \tag{70}$$

where the substitution $p - m = t$ has been utilized.

E. PROOF OF PROPERTY 5

For the first relation,

$$\begin{aligned} \left|\sum_{n=0}^{M-1} g[m,n]\right| &= \left|\sum_{n=0}^{M-1}\frac{1}{M}\sum_{k=0}^{M-1} e^{-j\frac{2\pi}{M}m\pi[k]} e^{j\frac{2\pi}{M}nk}\right| \\ &= \left|\frac{1}{M}\sum_{k=0}^{M-1} e^{-j\frac{2\pi}{M}m\pi[k]} \sum_{n=0}^{M-1} e^{j\frac{2\pi}{M}nk}\right| \\ &= \left|\sum_{k=0}^{M-1} e^{-j\frac{2\pi}{M}m\pi[k]}\delta[k]\right| \\ &= \left|e^{-j\frac{2\pi}{M}m\pi[0]}\right| \\ &= 1 \end{aligned} \tag{71}$$

$$\left|\sum_{m=0}^{M-1} g[m,n]\right| = \left|\sum_{m=0}^{M-1}\frac{1}{M}\sum_{k=0}^{M-1} e^{-j\frac{2\pi}{M}m\pi[k]} e^{j\frac{2\pi}{M}nk}\right|$$

$$= \left| \frac{1}{M} \sum_{k=0}^{M-1} e^{j\frac{2\pi}{M}nk} \sum_{m=0}^{M-1} e^{-j\frac{2\pi}{M}m\pi[k]} \right|$$
$$= \left| \sum_{k=0}^{M-1} e^{j\frac{2\pi}{M}nk} \delta[\pi[k]] \right|$$
$$= \left| e^{j\frac{2\pi}{M}nk'} \right|$$
$$= 1 \tag{72}$$

where $\pi[k'] = 0$.

For the second relation, it follows from (24) that $\sum_{n=0}^{M-1} |g[m,n]|^2 = \rho_{g_m g_m}[0] = 1$. Furthermore,

$$\sum_{m=0}^{M-1} |g[m,n]|^2 = \sum_{m=0}^{M-1} \frac{1}{M} \sum_{k=0}^{M-1} e^{-j\frac{2\pi}{M}m\pi[k]} e^{j\frac{2\pi}{M}nk} \times \frac{1}{M} \sum_{p=0}^{M-1} e^{j\frac{2\pi}{M}m\pi[p]} e^{-j\frac{2\pi}{M}np}$$
$$= \frac{1}{M^2} \sum_{k=0}^{M-1} \sum_{p=0}^{M-1} e^{j\frac{2\pi}{M}n(k-p)} \sum_{m=0}^{M-1} e^{j\frac{2\pi}{M}m(\pi[p]-\pi[k])}$$
$$= \frac{1}{M} \sum_{k=0}^{M-1} 1$$
$$= 1 \tag{73}$$

since the last sum is equal to M when $\pi[p] = \pi[k]$, which implies that $k = p$.

F. PROOF OF PROPERTY 6

From (6), the basis function with an LPP can for $N = M$ be simplified as

$$g[m,n] = \frac{1}{M} \sum_{k=0}^{M-1} e^{-j\frac{2\pi}{M}m(f_1 k + f_0)} e^{j\frac{2\pi}{M}nk}$$
$$= e^{-j\frac{2\pi}{M}mf_0} \frac{1}{M} \sum_{k=0}^{M-1} e^{j\frac{2\pi}{M}k(n-mf_1)}$$
$$= e^{-j\frac{2\pi}{M}mf_0} \delta\big[n - mf_1 \ (\mathrm{mod}\, M)\big]. \tag{74}$$

Therefore, $u(|g[m,n]|) = 1$ when $n \equiv mf_1 \ (\mathrm{mod}\, M)$. which implies that there is one sample n_0 per basis function m for which $g[m,n_0] \neq 0$ and it thus follows that $V = M$.

G. PROOF OF PROPERTY 7

The basis function is defined as

$$g[m,n] = e^{-j\frac{2\pi}{M}f_0 m} \sum_{k=0}^{M-1} e^{j\frac{2\pi}{M}k(n-mf_1-kmf_2)}. \tag{75}$$

Suppose M is even, $a = 0, 1$ and $b = 0, 1, \ldots, M/2-1$. Substituting $k = \frac{M}{2}a + b$ in (75), gives

$$g[m,n] = e^{-j\frac{2\pi}{M}f_0 m} \sum_{a=0}^{1} \sum_{b=0}^{M/2-1} e^{j\frac{2\pi}{M}\left(\frac{M}{2}a+b\right)\left(n-mf_1-\left(\frac{M}{2}a+b\right)mf_2\right)}$$
$$= e^{-j\frac{2\pi}{M}f_0 m} \sum_{a=0}^{1} e^{-j2\pi\left(mf_2\left(\frac{M}{4}a^2+ab\right)+\frac{mf_1-n}{2}a\right)} \times \sum_{b=0}^{M/2-1} e^{j\frac{2\pi}{M}b(n-mf_1-bmf_2)}$$
$$= e^{-j\frac{2\pi}{M}f_0 m}\left(1 + e^{-j\pi\left(mf_2\frac{M}{2}+mf_1-n\right)}\right) \times \sum_{b=0}^{M/2-1} e^{j\frac{2\pi}{M}b(n-mf_1-bmf_2)}. \tag{76}$$

Thus, from (76) it can be observed that if $v = m_0 f_2 \frac{M}{2} + m_0 f_1 - n_0$ is an odd integer, then $g[m_0, n_0] = 0$. Furthermore, for a given basis function m_0, $m_0 f_1 + m_0 f_2 \frac{M}{2}$ is fixed, thus every other value of v will be an odd integer. Hence, the number of non-zero elements of $g[m,n]$ is upper bounded by $M/2$. Moreover, it follows from (6) that $g[0,n] = \delta[n], \forall n$. Thus, $V \leq (M-1)M/2 + 1$.

H. PROOF OF PROPERTY 8

For any integers a and b,

$$e^{-j\frac{2\pi}{M}(ak^2+bk)} = e^{-j\frac{2\pi}{M}(a(k+M)^2+b(k+M))} \tag{77}$$

thus, it follows that

$$\sum_{k=0}^{M-1} e^{-j\frac{2\pi}{M}(ak^2+bk)} = \sum_{k=0}^{M-1} e^{-j\frac{2\pi}{M}(a(k+d)^2+b(k+d))} \tag{78}$$

for any integer d. Let $D = \gcd(a, M) > 1$ and $d = M/D$. Then, (78) gives

$$\sum_{k=0}^{M-1} e^{-j\frac{2\pi}{M}(ak^2+bk)} = \sum_{k=0}^{M-1} e^{-j\frac{2\pi}{M}\left(ak^2+bk+a\left(2k\frac{M}{D}+\left(\frac{M}{D}\right)^2\right)+\frac{M}{D}b\right)}$$
$$= e^{-j2\pi\frac{b}{D}} \sum_{k=0}^{M-1} e^{-j\frac{2\pi}{M}(ak^2+bk)} \tag{79}$$

where the last step follows from that a/D and M/D are integers. Thus, if $D \nmid b$, then $e^{-j2\pi\frac{b}{D}} \neq 1$, which implies that

$$\sum_{k=0}^{M-1} e^{-j\frac{2\pi}{M}(ak^2+bk)} = 0. \tag{80}$$

From (18), it follows that $a = mf_2$ and $b = mf_1 - n$, and thus if

$$\gcd(m_0 f_2, M) \nmid m_0 f_1 - n_0 \tag{81}$$

then $g[m_0, n_0] = 0$.

I. PROOF OF PROPERTY 9

The relation between basis functions for a permutation polynomial $\pi[k]$ and its associated inverse permutation polynomial, $\pi^{-1}[k]$ is,

$$g_\pi[m,n] = \frac{1}{M} \sum_{k=0}^{M-1} e^{-j\frac{2\pi}{M}m\pi[k]} e^{j\frac{2\pi}{M}nk}$$

$$= \frac{1}{M}\sum_{p=0}^{M-1} e^{-j\frac{2\pi}{M}mp} e^{j\frac{2\pi}{M}n\pi^{-1}[p]}$$
$$= g^*_{\pi^{-1}}[n,m] \tag{82}$$

where the second step follows from variable substitution $p = \pi[k]$. Therefore, from (82) it follows that

$$\begin{aligned} V_{\pi^{-1}} &= \sum_{m=0}^{M-1}\sum_{n=0}^{M-1} u\big(|g_{\pi^{-1}}[m,n]|\big) \\ &= \sum_{m=0}^{M-1}\sum_{n=0}^{M-1} u\big(|g^*_{\pi}[n,m]|\big) \\ &= \sum_{m=0}^{M-1}\sum_{n=0}^{M-1} u(|g_{\pi}[n,m]|) \\ &= \sum_{m=0}^{M-1}\sum_{n=0}^{M-1} u(|g_{\pi}[m,n]|) \\ &= V_{\pi} \end{aligned} \tag{83}$$

which implies the same value V.

J. DERIVATION OF (31)

From the definition (6), we obtain

$$\begin{aligned} |g[m,n]|^2 &= \frac{1}{M^2}\sum_{k=0}^{M-1}\sum_{s=0}^{M-1} e^{-j\frac{2\pi}{M}\left(mf_2k^2+(mf_1-n)k+mf_0\right)} \\ &\quad\times e^{j\frac{2\pi}{M}\left(mf_2s^2+(mf_1-n)s+mf_0\right)} \\ &= \frac{1}{M^2}\sum_{k=0}^{M-1}\sum_{s=0}^{M-1} e^{-j\frac{2\pi}{M}\left(mf_2\left(s^2-k^2\right)+(mf_1-n)(s-k)\right)} \\ &= \frac{1}{M^2}\sum_{k=0}^{M-1}\sum_{t=0}^{M-1} e^{-j\frac{2\pi}{M}(mf_2(2k+t)t+(mf_1-n)t)} \\ &= \frac{1}{M^2}\sum_{t=0}^{M-1} e^{-j\frac{2\pi}{M}(mf_2t^2+(mf_1-n)t}\sum_{k=0}^{M-1} e^{-j\frac{2\pi}{M}2mf_2tk} \\ &= \frac{1}{M}\sum_{t=0}^{M-1} e^{-j\frac{2\pi}{M}(mf_2t^2+(mf_1-n)t}\delta\big[2mf_2t\ (\mathrm{mod}\,M)\big] \end{aligned}$$

where the variable substitution $s - k = t$ has been utilized.

APPENDIX B

We assume that $N_{\mathrm{CP}} \geq \tau_{L-1}$ and the received signal in the frequency domain, after CP removal, can then be expressed on matrix form as

$$\mathbf{R} = \mathbf{W}_M\mathbf{H}\mathbf{W}_M^{\dagger}\mathbf{P}\mathbf{W}_M\mathbf{x} + \tilde{\boldsymbol{\eta}} \tag{84}$$

where $\tilde{\boldsymbol{\eta}}$ is additive white Gaussian noise (AWGN) and $\mathbf{H}$ is the channel convolution matrix, which for a time-varying channel does not become circulant [33] and thus $\mathbf{W}_M\mathbf{H}\mathbf{W}_M^{\dagger}$ is not a diagonal matrix. We assume equalization by a MMSE filter, i.e., for a given SNR, $\mathbf{E} = ((\mathbf{W}_M\mathbf{H}\mathbf{W}_M^{\dagger})^{\dagger}\mathbf{W}_M\mathbf{H}\mathbf{W}_M^{\dagger} + \mathrm{SNR}^{-1}\,\mathbf{I})^{-1}(\mathbf{W}_M\mathbf{H}\mathbf{W}_M^{\dagger})^{\dagger}$, where detection is made from $\hat{\mathbf{x}} = \mathbf{W}_M^{\dagger}\mathbf{P}^{-1}\mathbf{E}\mathbf{R}$.

REFERENCES

[1] R. He, F. Bai, G. Mao, J. Härri, and P. Kyösti, "Guest editorial 5G wireless communications with high mobility," *IEEE J. Sel. Areas Commun.*, vol. 38, no. 12, pp. 2717–2722, Dec. 2020.

[2] J. Wu and P. Fan, "A survey on high mobility wireless communications: Challenges, opportunities and solutions," *IEEE Access*, vol. 4, pp. 450–476, 2016.

[3] "Solutions for NR to support non-terrestrial networks (NTN) (Release 16)," 3GPP, Sophia Antipolis, France, Rep. TR 38.821, V16.0.0, Dec. 2019. [Online]. Available: https: www.3gpp.org

[4] "Study on scenarios and requirements for next generation access technologies; (release 16)," 3GPP, Sophia Antipolis, France, Rep. TR 38.913, V16.0.0, Jul. 2020. [Online]. Available: https: www.3gpp.org

[5] T. Levanen, O. Tervo, K. Pajukoski, M. Renfors, and M. Valkama, "Mobile communications beyond 52.6 GHz: Waveforms, numerology, and phase noise challenge," *IEEE Wireless Commun.*, vol. 28, no. 1, pp. 128–135, Feb. 2021.

[6] S. Tarboush, H. Sarieddeen, M.-S. Alouini, and T. Y. Al-Naffouri, "Single- versus multicarrier terahertz-band communications: A comparative study," *IEEE Open J. Commun. Soc.*, vol. 3, pp. 1466–1486, 2022.

[7] H. S. Eshwaraiah and A. Chockalingam, "SC-FDMA for multiuser communication on the downlink," in *Proc. 5th Int. Conf. Commun. Syst. Netw. (COMSNETS)*, Bangalore, India, 2013, pp. 1–7.

[8] F. Berggren and B. M. Popović, "Chirp convolved data transmission," *IEEE Commun. Lett.*, vol. 25, no. 4, pp. 1226–1230, Apr. 2021.

[9] F. Berggren and B. M. Popović, "Waveform based on ZAC sequences," in *Proc. IEEE Veh. Technol. Conf.*, Helsinki, Finland, Jun. 2022, pp. 1–6.

[10] O. Mauritz and B. M. Popović, "Optimum family of spectrum-shaping functions for PAPR reduction of DFT-spread OFDM signals," in *Proc. IEEE Veh. Technol. Conf.*, Montreal, QC, Canada, Sep. 2006, pp. 1–5.

[11] I. S. Nasarre, T. Levanen, K. Pajukoski, A. Lehti, E. Tiirola, and M. Valkama, "Enhanced uplink coverage for 5G NR: Frequency-domain spectral shaping with spectral extension," *IEEE Open J. Commun. Soc.*, vol. 2, pp. 1188–1204, 2021.

[12] C. H. G. Yuen and B. Farhang-Boroujeny, "Analysis of the optimum precoder in SC-FDMA," *IEEE Trans. Wireless Commun.*, vol. 11, no. 11, pp. 4096–4107, Nov. 2012.

[13] K. Wu, G. Ren, X. Meng, J. Wu, and Q. Wang, "Spectral-efficient band allocation scheme for frequency-domain pulse-shaping-based SC-FDMA systems," *IEEE Trans. Veh. Technol.*, vol. 66, no. 9, pp. 8249–8262, Sep. 2017.

[14] A. Şahin, N. Hosseini, H. Jamal, S. S. M. Hoque, and D. W. Matolak, "DFT-spread-OFDM based chirp transmission," *IEEE Commun. Lett.*, vol. 25, no. 3, pp. 902–906, Mar. 2021.

[15] A. Bemani, N. Ksairi, and M. Kountouris, "AFDM: A full diversity next generation waveform for high mobility communications," in *Proc. IEEE Int. Conf. Commun. Workshops (ICC Workshops)*, Montreal, QC, Canada, Jun. 2021, pp. 1–6.

[16] W. Wang, X. Gao, X. You, and K.-K. Wong, "Frequency-interleaved DFT-spread OFDM transmission with an iterative receiver," in *Proc. IEEE Int. Conf. Wireless Commun. Signal Process.*, Nanjing, China, Nov. 2009, pp. 1–5.

[17] G. Stolfi and L. A. Baccala, "Fourier transform time interleaving in OFDM modulation," in *Proc. IEEE Ninth Int. Symp. Spread Spectr. Techn. Appl.*, Manaus, Brazil, Aug. 2006, pp. 158–162.

[18] J. Lahtonen, J. Ryu, and E. Suvite, "On the degree of the inverse of quadratic permutation polynomial interleavers," *IEEE Trans. Inf. Theory*, vol. 58, no. 6, pp. 3925–3932, Jun. 2012.

[19] E. Nieminen, "On quadratic permutation polynomials, turbo codes, and butterfly networks," *IEEE Trans. Inf. Theory*, vol. 63, no. 9, pp. 5793–5801, Sep. 2017.

[20] C. Xiao, Y. R. Zheng, and N. C. Beaulieu, "Novel sum-of-sinusoids simulation models for Rayleigh and Rician fading channels," *IEEE Trans. Wireless Commun.*, vol. 5, no. 12, pp. 3667–3679, Dec. 2006.

[21] L. Trifina and D. Tarniceriu, "A simple method to determine the number of true different quadratic and cubic permutation polynomial based interleavers for turbo codes," *Telecommun. Syst.*, no. 64, pp. 147–171, May 2017.

[22] O. Y. Takeshita, "Permutation polynomial interleavers: An algebraic-geometric perspective," *IEEE Trans. Inf. Theory*, vol. 53, no. 6, pp. 2116–2132, Jun. 2007.

[23] E. Rosnes, "On the minimum distance of turbo codes with quadratic permutation polynomial interleavers," *IEEE Trans. Inf. Theory*, vol. 58, no. 7, pp. 4781–4795, Jul. 2012.
[24] H. Zhao, P. Fan, and V. Tarokh, "On the equivalence of interleavers for turbo codes using quadratic permutation polynomials over integer rings," *IEEE Commun. Lett.*, vol. 14, no. 3, pp. 236–238, Mar. 2010.
[25] *Physical Channels and Modulation; (Release 17)*, 3GPP Standard TS 38.211, V17.4.0, Dec. 2022. [Online]. Available: https: www.3gpp.org
[26] *Multiplexing and Channel Coding; (Release 17)*, 3GPP Standard TS 38.212, V17.4.0, Dec. 2022. [Online]. Available: https: www.3gpp.org
[27] B. Yuan and K. K. Parhi, "Successive cancellation list polar decoder using log-likelihood ratios," in *Proc. 48th Asilomar Conf. Signals, Syst. Comput.*, Pacific Grove, CA, USA, Nov. 2014, pp. 548–552.
[28] "Study on physical layer enhancements for NR ultra-reliable and low latency case (URLLC); (release 16)," 3GPP, Sophia Antipolis, France, Rep. TR 38.824, V16.0.0, Mar. 2019. [Online]. Available: https: www.3gpp.org
[29] M. Sharif, M. Gharavi-Alkhansari, and B. H. Khalaj, "On the peak-to-average power of OFDM signals based on oversampling," *IEEE Trans. Commun.*, vol. 51, no. 1, pp. 72–78, Jan. 2003.
[30] L. Cho, Y.-M. Kuo, and C.-Y. Hsu, "Rotated DFT-spread OFDM for low-PAPR transmission," in *Proc. IEEE 3rd Int. Conf. Commun. Inf. Syst. (ICCIS)*, Singapore, Dec. 2018, pp. 146–149.
[31] R. G. Bohórquez, C. A. Nour, and C. Douillard, "On the equivalence of interleavers for turbo codes," *IEEE Wirelss Commun. Lett.*, vol. 4, no. 1, pp. 59–61, Feb. 2015.
[32] P. J. S. G. Ferreira, "A group of permutations that commute with the discrete Fourier transform," *IEEE Trans. Signal Process.*, vol. 42, no. 2, pp. 444–445, Feb. 1994.
[33] M. Guillaud and D. T. M. Slock, "Channel modeling and associated inter-carrier interference equalization for OFDM systems with high Doppler spread," in *Proc. IEEE Int. Conf. Acoust., Speech, Signal Process.*, Apr. 2003, pp. 237–240.

FREDRIK BERGGREN (Senior Member, IEEE) received the M.Sc. degree in applied physics and electrical engineering from Linköping University, Sweden, in 1998, and the Ph.D. degree in electrical engineering from the Royal Institute of Technology, Sweden, in 2003. Since 2005, he has been with Huawei Technologies, Stockholm, Sweden, where he holds the position as an Expert. He has participated in 3GPP RAN1 for more than a decade and has contributed to physical layer standardization of Long Term Evolution (LTE), its successor LTE-Advanced, and 5G New Radio. He is the inventor of numerous standard-essential patents. His research interests include radio access networks, with emphasis on physical layer waveforms, channels, and procedures. He has received several awards for his contributions to Huawei's patent portfolio. He is a co-recipient of the IEEE Communications Society Heinrich Hertz Award for Best Communications Letter in 2010.

BRANISLAV M. POPOVIĆ received the Ph.D. degree in electrical engineering from the School of Electrical Engineering, University of Belgrade, Serbia. Prior to joining Huawei Technologies, Stockholm, Sweden, in 2001, he was with the Institute of Microwave Techniques and Electronics, Belgrade, from 1984 to 1994, Ericsson, Stockholm, from 1994 to 2000, and Marconi, Stockholm, from 2000 to 2001. He is a Huawei Fellow.